The Astrophysical Journal, 895:108 (11pp), 2020 June 1 https://doi.org/10.3847/1538-4357/ab8d26

Counting on Short Gamma-Ray Bursts: Gravitational-wave Constraints of Jet Geometry

Amanda Farah[1], Reed Essick[2,3], Zoheyr Doctor[1,4], Maya Fishbach[5], and Daniel E. Holz[1,5,2,3]
[1] Department of Physics, University of Chicago, Chicago, IL 60637, USA
[2] Kavli Institute for Cosmological Physics, University of Chicago, Chicago, IL 60637, USA
[3] Enrico Fermi Institute, University of Chicago, Chicago, IL 60637, USA
[4] Department of Physics, University of Oregon, Eugene, OR 97403, USA
[5] Department of Astronomy and Astrophysics, University of Chicago, Chicago, IL 60637, USA
Received 2020 February 10; revised 2020 April 16; accepted 2020 April 25; published 2020 June 2

Abstract

The detections of GW170817 and GRB 170817A revealed that at least some short gamma-ray bursts (sGRB) are associated with the merger of neutron-star compact binaries. The gamma-rays are thought to result from the formation of collimated jets, but the details of this process continue to elude us. One important feature of gamma-ray bursts is the emission profile of the jet as a function of viewing angle. We present two related methods to measure the effective angular width, θ_B, of sGRB jets using gravitational-wave (GW) and gamma-ray data, assuming all sGRBs have the same angular dependence for their luminosities. The first is a counting experiment that requires minimal knowledge about each event, beyond whether or not they were detected in gamma-rays. The second method uses GW and electromagnetic data to estimate parameters of the source. We additionally outline a model-independent method to infer the full jet structure of sGRBs using a nonparametric approach. Applying our methods to GW170817 and GW190425, we find weak constraints on the sGRB luminosity profile. We project that with 5 and 100 binary neutron star detections, the counting method would constrain the relative uncertainty in θ_B to within 51% and 12%, respectively. Incorporating GW parameter estimation provides only marginal improvements. We conclude that the majority of the information about jet structure comes from the relative sensitivities of GW and gamma-ray detectors as encoded in simple counting experiments.

Unified Astronomy Thesaurus concepts: Neutron stars (1108); Gamma-ray bursts (629); Gravitational waves (678)

1. Introduction

Because of their scarcity, irregularity, and brevity, very little is known about the origin and formation mechanisms of short gamma-ray bursts (sGRBs). Though it was postulated for decades that sGRBs could result from the mergers of binary neutron star (BNS) systems (e.g., Eichler et al. 1989; Narayan et al. 1992; Fong et al. 2010; Church et al. 2011) or neutron star–black hole systems (see Berger 2014 for a recent review), the joint gamma-ray and gravitational-wave detection of GW170817 confirmed this association observationally for the first time (Abbott et al. 2017a, 2017b; Wu & MacFadyen 2019; Goldstein et al. 2017; Savchenko et al. 2017). Indeed, this breakthrough was only possible by simultaneously observing the multimessenger sky with the Fermi Gamma-Ray Burst Monitor (GBM, Meegan et al. 2009) and the advanced LIGO (Aasi et al. 2015) and Virgo (Acernese et al. 2015) gravitational-wave (GW) detectors. However, there still remain many open questions about the mechanism by which gamma-rays are generated. A property of sGRBs that is sensitive to the underlying astrophysics of the merger is the angular structure of the gamma-ray emission. Thus, understanding this structure may lead to insights about the generation mechanism of gamma-rays (Aloy et al. 2005; Nagakura et al. 2014; Kumar & Zhang 2015).

Although the specific angular geometry of sGRB jets is unknown, there are several features believed to be common to these phenomena. First, sGRB jets are thought to be launched from the poles of the remnant left over after the coalescence of two neutron stars or a neutron star and a black hole. The precise mechanism by which the jet is launched is still unknown (Berger 2014, but see also Liu et al. 2015 and references therein), but it is generally believed that there are symmetric polar outflows of highly relativistic material that travel parallel to the binary system's orbital angular momentum. Furthermore, jets are thought to be collimated and roughly axisymmetric, emitting preferentially in a narrow opening angle due to a combination of outflow geometry and relativistic beaming. Importantly, the angular dependence of the jet luminosity is very uncertain. We assume it decreases monotonically at large viewing angles (off-axis) compared to lines of sight nearly aligned with the progenitor system's angular momentum (on-axis). This means that the majority of sGRBs are only detectable if they are aligned within a narrow window around our line of sight, although off-axis detection is still plausible if the source is at sufficiently low redshift (Metzger & Berger 2012; Lazzati et al. 2017). This could explain why GRB 170817A was highly subluminous, although it has been argued that it might instead be a member of a separate subluminous population of sGRBs (Siellez et al. 2016; Abbott et al. 2017a). GW radiation from the sGRB progenitor, although still preferentially emitted along the orbit's angular momentum, has a much shallower angular dependence. These systems are therefore detectable in GWs at much larger viewing angles than sGRBs. We investigate the interplay between the different angular scales in sGRB and GW emission profiles, following up on previous counting experiments (e.g., Chen & Holz 2013; Nagakura et al. 2014) and investigating the impact of additional information beyond the relative sensitivities of GW and gamma-ray detectors.

We present two methods to infer the geometrical properties of sGRB emission by relating parameters that can be extracted from the GW signal, such as the inclination and redshift of the system, to the number of sGRBs detected. We also make a prediction for the constraining power of these methods, and

show that, in an optimistic scenario of 100 BNS detections and a tophat jet structure, the beaming angle will be constrained to within 2.7° if $\leqslant 20$ of these events have associated sGRBs. In addition, we find that the ability to constrain jet structure is relatively model independent. Incorporating GW measurements of the systems' inclinations will initially help constrain jet structure, although the basic counting experiment will produce nearly equivalent constraints by the time modeling systematics dominate over statistical uncertainty.

The framework presented here is complementary to current methods that consider only EM data and infer beaming angles for each sGRB through radio afterglow observations (Fong et al. 2015; Ghirlanda et al. 2016). Radio afterglow measurements employ the fact that a jet break occurs when the relativistic Lorentz factor (Γ) approaches $\sim\theta_B^{-1}$, resulting in a characteristic steepening of the light curve (Jin et al. 2018; Wang et al. 2018). Given a model for the evolution of Γ over time (e.g., Blandford & McKee 1976; Suzuki & Shigeyama 2014), one can then deduce the beaming angle using the time between gamma-ray emission and jet break. Thus, an independent measurement of the beaming angle would enable progress on the reverse problem, allowing for insights on the energetics of the burst (Frail et al. 2001; Nagakura et al. 2014; Yi et al. 2017). Instead of inferring jet structure parameters for individual sGRBs (Laskar et al. 2016, 2018; Zhang 2016; Gill & Granot 2018; Lyman et al. 2018; Zou et al. 2018), we consider the population of sGRBs that are accompanied by GWs and constrain the beaming angle with observations of multiple sGRBs.

Other studies have investigated similar relationships. For example, Mogushi et al. (2019) take a sample of sGRBs with known luminosities and infer a rate of BNS mergers for several choices of luminosity functions. Assuming a universal structured jet in the form of a broken power law, they constrain the jet parameters based on GW170817 (Abbott et al. 2017b) and their sGRB sample. Using these two measurements, they infer an expected rate of *coincident* gamma-ray bursts and GW detections.

We solve a related problem. Through a simple counting experiment that expands on the work in Chen & Holz (2013), we constrain sGRB jet parameters by using the number of sGRBs detected in coincidence with BNS mergers detected in GWs. Instead of predicting the rate of coincident detections based on a model of the jet structure, we study how well jet structures can be constrained given a set of coincident detections. To do this, we sample BNS systems from a physically motivated redshift, inclination, and maximum luminosity distribution. Then, taking advantage of the redshift and inclination dependence of both GW detector and GBM sensitivities, we determine the likelihood of detecting BNSs in GWs with and without associated sGRBs as a function of θ_B. We examine various two-parameter jet structure models in this way. Additionally, we show how to easily extend this analysis to include posterior distributions from GW data when available.

Biscoveanu et al. (2020) and Hayes et al. (2020) have recently presented similar studies. We highlight a number of important differences with their work. First, neither Biscoveanu et al. (2020) nor Hayes et al. (2020) consider selection effects, whereas this work shows that knowledge of selection effects leads to constraints on the jet width that are comparable to those obtained from GW parameter estimation. Second, both Biscoveanu et al. (2020) and Hayes et al. (2020) parameterize the fluence of gamma-rays in terms of the jet structure models that they consider, whereas this work only considers luminosity to the extent that events are above the GBM threshold. The methods in Biscoveanu et al. (2020) and Hayes et al. (2020) therefore require additional information from the gamma-ray detection, beyond what is assumed in the methods we present.

Additionally, Hayes et al. (2020) focuses mainly on model selection between two jet structures. It discusses the number of events it would take to distinguish between jet structures. We make no such attempt, but show that different jet structures can produce different constraints. Biscoveanu et al. (2020) assume a joint detection or the availability of a fluence upper limit and employ parameter estimation to obtain posteriors for gravitational-wave and electromagnetic counterpart parameters. This necessitates simulating 200 BNS merger events, specifying waveform models, and injecting these events into LIGO detector networks.

The work presented here takes a simpler approach, where the posterior on jet width given the number of GW and sGRB detections is analytically derived and then calculated by sampling from priors on inclination and redshift. To incorporate parameter estimation information, one directly applies posterior samples from the publicly available gravitational-wave transient catalogs (Abbott et al. 2019a). Perhaps surprisingly, this straightforward approach appears to be as effective as those presented in Biscoveanu et al. (2020) and Hayes et al. (2020), as all three studies determine the beaming angle with errors of less than $\sim$10° after 100 events.

We make several simplifying assumptions for the physical properties of sGRBs as well as their detection criteria. First, we only consider detections from GBM, which is sensitive to $\sim$70% of the sky (the other $\sim$30% is occulted by the Earth) and only observes for 85% of the time. The parts of the sky to which GBM and LIGO/Virgo are sensitive at any moment are not believed to be correlated as the typical lock duration of GW interferometers (The LIGO Scientific Collaboration 2019) is much longer than Fermi's orbital period ($\sim$96 minutes; Meegan et al. 2009). Sky coverage from other instruments like Swift-BAT (Gehrels et al. 2004) and Konus-Wind (Aptekar et al. 1995) are negligible in comparison.

Second, we assume that matter ejected from a BNS merger emits radiation in the form of two axisymmetric jets of gamma-rays that are aligned with the system's angular momentum. Thus, the inclination ι of the BNS relative to our line of sight is a perfect proxy for viewing angle, and we will make no distinction between the two. Third, we assume that all BNS mergers result in an sGRB.

Fourth, and least conventional, is our assumption that sGRBs have a universal jet structure. We choose structures that monotonically decrease with increasing viewing angle and that are described by only two free parameters. A universal jet structure $\mathcal{L}(\iota; \theta_B, L_{\max})$ implies that the observed isotropic equivalent luminosity of a given sGRB depends only on the viewing angle (ι) of the observer, up to an overall scaling constant ($L_{\max}$). We consider three functional forms for the luminosity of the jet as function of viewing angle: a tophat, a broken power law, and a Gaussian. In all three jet models, the two parameters are the width of the jet (θ_B) and the luminosity at the very center of the jet ($L_{\max}$). While not guaranteed to be the case, this assumption is motivated by Wu & MacFadyen (2019), who argue that all cosmological sGRBs have the same afterglow, and differences in afterglow are due to different

viewing angles and distances. It is thus not unreasonable to postulate that the same might be true for the prompt gamma-ray emission, as it is certainly plausible that the prompt emission structure is related to the afterglow structure. Additionally, Perna et al. (2003) show that a universal structured jet model of sGRBs is consistent with the observed distribution of viewing angles. Nakar et al. (2004) argue that this statement is not valid for the 2D distribution of viewing angles and redshift, but note that any disagreement might be due to inhomogeneity in sGRB observations or selection effects. Thus, it is not unreasonable to assume a universal structure for sGRB jets with the caveat that, if this assumption does not hold, any measurement of jet parameters that relies on detections of multiple jets with the same parameters would have to be reassessed.

Within these jet structure models is the simplifying assumption that all effects on the observed luminosity of an sGRB due to Lorentz factor variation and the jet's energy structure can be captured in the angular dependence of the jet's luminosity. However, some jet structure models are not sufficient at characterizing all of the possible effects that can arise. For example, models that have a sharp truncation at higher viewing angles are not possible if the Lorentz factor falls off at the jet wings. Thus, higher-parameter jet structure models than the ones used here may be necessary to fully account for these effects. An extensive discussion of such effects can be found in Salafia et al. (2015).

We investigate the implications of these four assumptions for future jet structure constraints.

This paper is organized as follows. Section 2 details the method used to infer jet parameters from GW-only and joint sGRB-GW detections of BNS mergers, and Section 2.3 explains how one would extend this method to include information from GW parameter estimation. Section 3 summarizes the results and provides predicted constraints from future detections. We conclude by discussing this method's limitations and outlining other possible approaches in Section 4.

2. Methods

We carry out a Bayesian analysis to infer the width of sGRB jets from a BNS merger for three structured jet models. There are several naming conventions in the field, so we first define our parameters.

1. $N_{\rm GW}$ and $N_{\rm coinc}$ are the number of BNS mergers detected in GWs and the number of sGRBs detected by GBM in coincidence with a GW detection, respectively. Therefore, $0 \leqslant N_{\rm coinc} \leqslant N_{\rm GW}$.
2. $\mathcal{L}(\iota;\, \theta_B,\, L_{\rm max})$ is the isotropic equivalent luminosity as a function of viewing angle for *all* sGRBs. This is the function that describes the jet structure. We assume there is a universal angular dependence for all sGRBs, so that $\mathcal{L}/L_{\rm max}$ is the same for every jet.
3. θ_B is the width of the jet. For a tophat (Equation (6)), this is the half opening angle, beyond which no light is emitted. For $\theta_B = \pi/2$, each jet covers half the sky, and the gamma-rays are emitted isotropically. For a Gaussian jet (Equation (7)), θ_B is the standard deviation of the angular profile, and for a broken power law (Equation (8)), θ_B is the inclination at which the jet structure function is truncated, i.e., where the luminosity is set to zero. Note that the meaning of θ_B can be quite different for each jet structure model and one must take care when comparing model-dependent statements.
4. $L_{\rm max}$ is the luminosity at the center of the jet and can be thought of as the overall normalization of the jet structure. In this work, we draw $L_{\rm max}$ from a log-normal distribution with mean 5×10^{51} erg s^{-1} and width 0.56 dex, following Salafia et al. (2015). This distribution was chosen to be consistent with the majority of observed sGRBs with known redshift (see Figure 4 of Abbott et al. 2017a). Note that even though the angular dependence of the jet luminosity is assumed to be universal, drawing $L_{\rm max}$ from a distribution allows for variations in the overall luminosity of different sGRBs, which could be due to different energy reservoirs in the remnants or different component masses in the progenitor systems.
5. $L_{\rm iso}$ is the isotropic equivalent luminosity of an sGRB. Isotropic energetics are calculated under the assumption that the source emits isotropically, so that the luminosity in the observer's direction is the luminosity everywhere. This is often considered an upper bound on the true total energetics if one assumes that the GRB is observed at the brightest part of the jet (Section 6.1 of Abbott et al. 2017a), although this is only true for a tophat jet structure.
6. ι is the viewing angle, or the inclination of the system relative to our line of sight. It is defined as the angle between our line of sight to the binary system and the system's angular momentum.
7. q is the coincident fraction, defined as the fraction of BNS mergers detected in GWs that also have an associated sGRB detected by GBM. Given the sensitivities of both detectors, the electromagnetic parameters of sGRBs, as well as an assumed distribution of BNS mergers in redshift and inclination, we calculate the coincident fraction in the limit of infinite detections:

$$q \equiv \lim_{N_{\rm GW}\to\infty} \frac{N_{\rm coinc}}{N_{\rm GW}}.$$

We then use this to infer a posterior distribution of the jet opening angle θ_B for a given jet structure $\mathcal{L}(\iota;\, \theta_B,\, L_{\rm max})$ based on a finite number of detections.

2.1. Bayesian Formulation

Our goal is to constrain the effective angular width of sGRB jets, θ_B. We calculate the posterior probability $p(\theta_B|N_{\rm coinc},\, N_{\rm GW})$ based on the number of sGRB and GW detections:

$$p(\theta_B|N_{\rm coinc},\, N_{\rm GW}) = \frac{p(N_{\rm coinc},\, N_{\rm GW}|\theta_B)p(\theta_B)}{p(N_{\rm coinc},\, N_{\rm GW})}. \quad (1)$$

We assume a uniform prior in θ_B, so the posterior is proportional to the likelihood. Note that the coincident fraction, q, can be computed from θ_B, so we can rewrite the likelihood as $p(N_{\rm coinc},\, N_{\rm GW}|q(\theta_B))$. Because the detection of a GRB is a Boolean outcome, this likelihood is a binomial distribution with success fraction q, number of trials $N_{\rm GW}$, and number of successes $N_{\rm coinc}$. Replacing the likelihood and priors with their

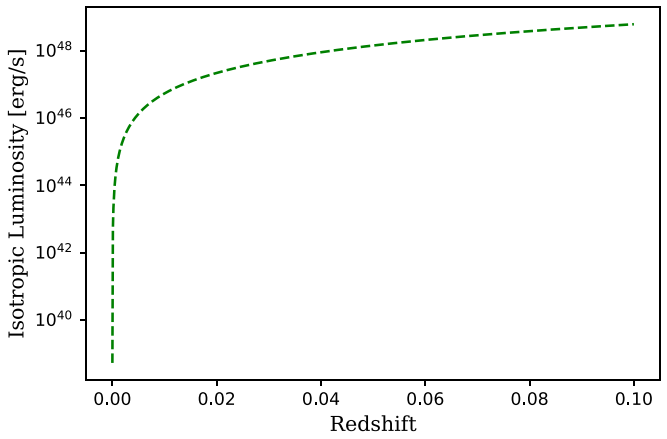

Figure 1. Approximate GBM isotropic luminosity detection threshold, $L_{\rm iso,thr}$, as a function of redshift, reproduced from Figure 4 of Abbott et al. (2017a). Note that this threshold increases slowly for $z \gtrsim 0.01$.

functional forms, we obtain

$$p(\theta_B|\ N_{\rm coinc}, N_{\rm GW}) = \frac{q(\theta_B)^{N_{\rm GW}}(1-q(\theta_B))^{N_{\rm GW}-N_{\rm coinc}}}{\int {\rm d}\theta_B q(\theta_B)^{N_{\rm GW}}(1-q(\theta_B))^{N_{\rm GW}-N_{\rm coinc}}}. \quad (2)$$

This shows that, for example, lower $N_{\rm coinc}$ and higher $N_{\rm GW}$ correspond to posterior support in a narrow region around small q and therefore small θ_B. This, then, reduces the problem of constraining the jet width to one of calculating the coincident fraction as a function of θ_B for a given jet structure.

2.2. Calculating the Coincident Fraction

The coincident fraction (q) is defined as the probability of detecting an sGRB given a BNS merger detection:

$$q = p(\mathcal{A}_{\rm coinc} = 1|\mathcal{A}_{\rm GW} = 1), \quad (3)$$

where $\mathcal{A}_{\rm coinc}$ ($\mathcal{A}_{\rm GW}$) is a Boolean indicator that represents whether or not the system was detected in gamma-rays (GWs). While individual detections depend on parameters such as source inclination and distance, we ultimately want q only as a function of the beaming angle θ_B and the maximum luminosity of the jet $L_{\rm max}$. Thus, to obtain $q(\theta_B)$, we marginalize over the unknown inclination angle ι and redshift z of a given system:

$$q = \int {\rm d}z{\rm d}\iota\ p(\mathcal{A}_{\rm coinc} = 1|\iota, z)p(\iota, z|\mathcal{A}_{\rm GW} = 1). \quad (4)$$

GBM detects an event when the observed flux is above a threshold, and a GRB's flux can be calculated from its equivalent isotropic luminosity $L_{\rm iso}$ and distance from Earth. Thus, GBM's flux threshold can be converted to an isotropic luminosity threshold as a function of redshift, as shown in Figure 1. We therefore write $p(\mathcal{A}_{\rm coinc}|\iota, z)$ as a function of $L_{\rm iso}$ and z:

$$p(\mathcal{A}_{\rm coinc} = 1|\iota, z) = f_{\rm vis.}\,\Theta(L_{\rm iso}(z, \iota) - L_{\rm iso,thr}(z)), \quad (5)$$

where $\Theta(x)$ is the Heaviside step function and $L_{\rm iso,thr}(z)$ is GBM's isotropic luminosity threshold at redshift z. $f_{\rm vis.}$ is the fraction of the sky to which GBM is sensitive. This is taken to be 0.7 since the Earth occults ~30% of GBM's field of view. However, this number can be modified to account for time spent in the South Atlantic Anomaly, as well as additional time for slewing and safe holding. For example, Burns et al. (2016) calculate a time-averaged sky fraction of ~0.6. The observed isotropic equivalent luminosity depends on the viewing angle and is given by the jet structure function $\mathcal{L}(\iota)$. We assume a universal jet structure, so $\mathcal{L}$ is known and is the same for all sGRBs. We consider tophat, ($\mathcal{L}_T$), Gaussian ($\mathcal{L}_G$), and broken power-law ($\mathcal{L}_P$) jets:

$$\mathcal{L}_T(\iota;\ \theta_B, L_{\rm max}) = L_{\rm max}\begin{cases}1 & \iota \leqslant \theta_B\\ 0 & \iota > \theta_B\end{cases} \quad (6)$$

$$\mathcal{L}_G(\iota;\ \theta_B, L_{\rm max}) = L_{\rm max}\, e^{-\frac{\iota^2}{2\theta_B^2}} \quad (7)$$

$$\mathcal{L}_P(\iota;\ \theta_B, L_{\rm max}) = L_{\rm max}\begin{cases}1 & \iota \leqslant \frac{\theta_B}{2}\\ \left(\frac{2\iota}{\theta_B}\right)^{-2} & \frac{\theta_B}{2} < \iota \leqslant \theta_B\\ 0 & \iota > \theta_B\end{cases}. \quad (8)$$

We note that the exponent in Equation (8) is fixed and is chosen for consistency with other studies (Zhang & Mészáros 2002; Wanderman & Piran 2015; Mogushi et al. 2019; Biscoveanu et al. 2020).

Now, we need the distribution of inclinations and redshifts given a GW detection, namely

$$p(\iota, z|\mathcal{A}_{\rm GW}) = \frac{p(\iota, z, \mathcal{A}_{\rm GW})}{p(\mathcal{A}_{\rm GW})} = \frac{p(\iota, z)p(\mathcal{A}_{\rm GW}|z, \iota)}{\int {\rm d}z{\rm d}\iota\ p(\mathcal{A}_{\rm GW}|z, \iota)p(\iota, z)},$$

given a GW selection function $p(\mathcal{A}_{\rm GW}|z, \iota)$ and a prior $p(\iota, z)$. We model the GW selection function assuming a single-detector signal-to-noise ratio threshold of $\rho_{\rm thr} = 8$. Thus, $p(\mathcal{A}_{\rm GW}|z, \iota) = \Theta(\rho(z, \iota) - \rho_{\rm thr})$ and we obtain

$$p(\iota, z|\mathcal{A}_{\rm GW}) = \frac{\Theta(\rho(z, \iota) - \rho_{\rm thr})p(\iota, z)}{\int {\rm d}z{\rm d}\iota\ \Theta(\rho(z, \iota) - \rho_{\rm thr})p(\iota, z)}. \quad (9)$$

Many factors contribute to an event's signal in a LIGO detector, such as the orientation of the source, distance to the source, and location of the source in the sky. A full explanation of these effects can be found in Finn & Chernoff (1993). A priori, we expect a BNS's redshift to be completely independent of its inclination with respect to Earth, so $p(\iota, z) = p(\iota)p(z)$. We further assume that in our detectable redshift range, BNS mergers are distributed uniformly in comoving volume V_c, so that

$$p(z) = p(V_c)\frac{{\rm d}V_c}{{\rm d}z} \propto \frac{{\rm d}V_c}{{\rm d}z}.$$

We adopt a ΛCDM cosmology with $H_0 = 70\,{\rm km\ s^{-1}\ Mpc^{-1}}$ and $\Omega_m = 0.3$. It is also safe to assume that the BNS inclinations are isotropically distributed. Thus,

$$p(\iota, z) \propto \frac{{\rm d}V_c}{{\rm d}z}\sin\iota. \quad (10)$$

Bringing this all together, we substitute Equations (5) and (9) into Equation (4) to obtain

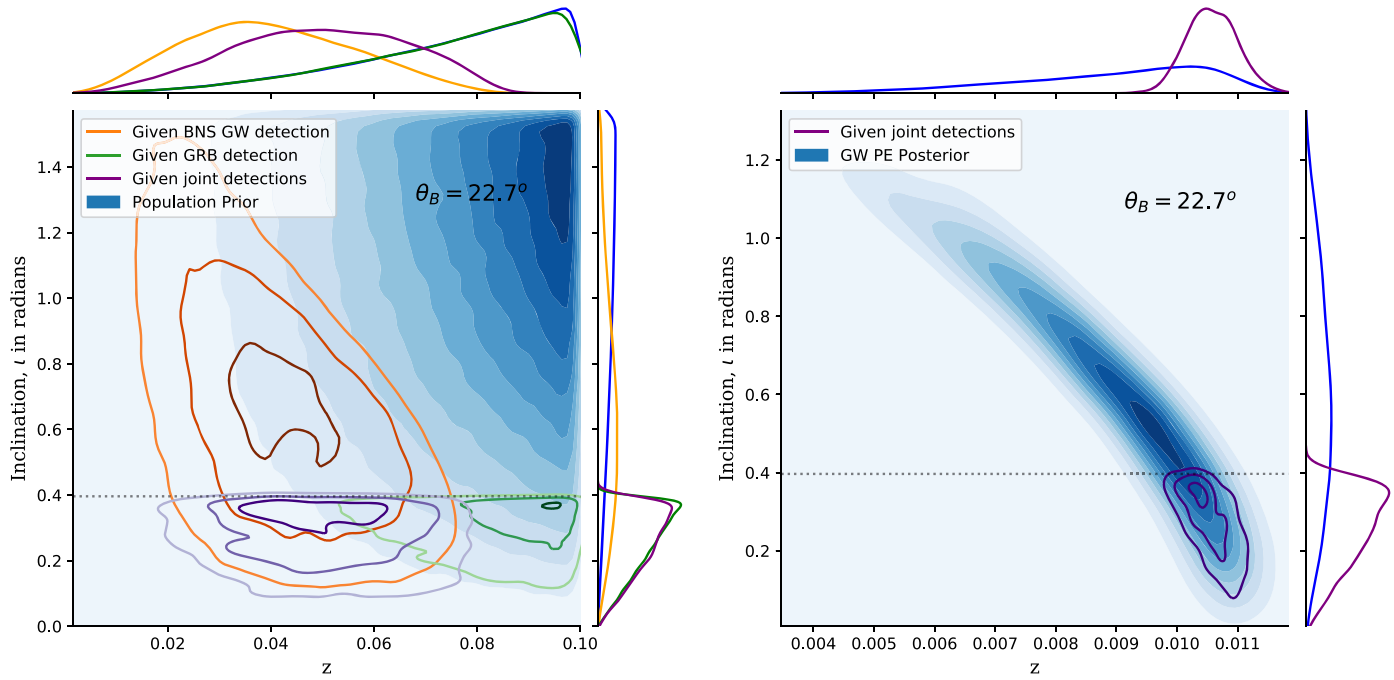

Figure 2. Illustration of selection effects with $\mathcal{O}(10^6)$ BNS systems uniformly distributed in comoving volume and isotropically oriented with tophat jets with $\theta_B = 22.7°$. Left: distributions without GW parameter estimation, as would be used in simple counting experiments. The prior $p(z, \iota)$ is shown in blue and the population of detected GW signals is in yellow. Right: the posterior distribution from GW170817, in which the blue shading acts like the yellow contours in the left panel. Note the different scales on both axes between the two panels. Both: the observed luminosity of each event is calculated for various values of θ_B (horizontal dashed gray line), and the population detected by GBM is shown with green contours. The population of joint detections is shown in purple contours. Contour levels are arbitrary and solely for illustrative purposes. In comparison to the GW distribution over z and ι without GW170817 parameter estimation, there is more support at lower inclination and lower redshift with parameter estimation (note that the limits on the horizontal axis in these figures differ by an order of magnitude). One would expect higher coincident fractions at a lower beaming angle than for the population prior. This can be seen in Figure 3.

$$q = f_{\text{vis.}} \frac{\int \mathrm{d}z\mathrm{d}\iota\, p(\iota, z)\Theta(\mathcal{L}(\iota; \theta_B, L_{\max}) - L_{\text{iso,thr}}(z))\Theta(\rho(z, \iota) - \rho_{\text{thr}})}{\int \mathrm{d}z\mathrm{d}\iota\, p(\iota, z)\Theta(\rho(z, \iota) - \rho_{\text{thr}})}, \tag{11}$$

which we evaluate with Monte-Carlo estimates of each integral, drawing $M = O(10^6)$ samples for z and ι from Equation (10) and drawing $L_{\max}$ from a log-normal distribution with mean 5×10^{51} erg s^{-1} and width 0.56 dex:

$$q \approx \frac{f_{\text{vis.}} \sum_{j=1}^{M} \Theta(\mathcal{L}(\iota_j; \theta_B, L_{\max}^{(j)}) - L_{\text{iso,thr}}(z_j))\Theta(\rho(\iota_j, z_j) - \rho_{\text{thr}})}{\sum_{j=1}^{M} \Theta(\rho(\iota_j, z_j) - \rho_{\text{thr}})}.$$

This looks like the ratio of coincident detections to all GW detections. This is illustrated in Figure 2. The population of sGRBs that would be detected varies drastically with different θ_B. The ratio of joint detections to GW-only detections has a maximum value of $f_{\text{vis.}}$ and is determined as a function of the beaming angle. This ratio, which is the coincident fraction $q(\theta_B)$, is shown in Figure 3.

Up until now, we have only considered the number of sGRBs observed in coincidence with a GW event. We relied on our knowledge of the selection effects of the detectors to provide information on the inclination and redshift of the BNS systems. However, detected systems provide additional information, since their parameters (such as redshift and inclination) can be estimated from the GW signal. Our simple counting experiment can be naturally extended to include this additional information, as we now demonstrate.

2.3. Including Information from GW Parameter Estimation

Consider an individual BNS merger, denoted by i, that is detected in GWs with data d_i. The coincident fraction for this event (q_i) is the likelihood of it being detected in gamma-rays given that it was detected in gravitational waves. We note that this quantity may be different for each event as we condition on different observed GW data. That is,

$$\begin{aligned} q_i &= p(\mathcal{A}^{(i)}_{\text{coinc}} | d_i, \mathcal{A}^{(i)}_{\text{GW}} = 1, \theta_B) \\ &= \frac{p(d_i, \mathcal{A}^{(i)}_{\text{coinc}}, \mathcal{A}^{(i)}_{\text{GW}} = 1 | \theta_B)}{p(d_i, \mathcal{A}^{(i)}_{\text{GW}} = 1)}. \end{aligned}$$

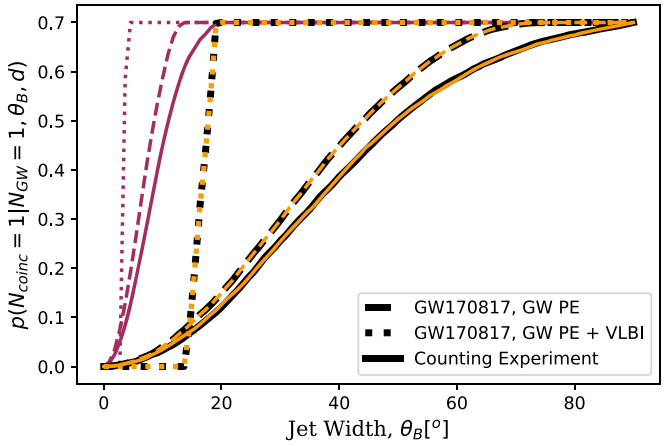

Figure 3. Coincident fraction $q(\theta_B) = p(N_{\rm coinc} = 1|N_{GW} = 1, \theta_B, d)$ as a function of θ_B with and without parameter estimation for GW170817. Given that a BNS was detected in GWs, the coincident fraction is the probability of detecting a coincident sGRB as a function of θ_B. If $q(\theta_B)$ is low for a given θ_B, that beaming angle is disfavored if a GW event event is accompanied by an sGRB detection. We show $q(\theta_B)$ for the tophat (black), broken power-law (orange), and Gaussian (violet) jet structure models with constraints from the counting experiment alone (solid), GW parameter estimation (dashed), and GW parameter estimation and very long baseline interferometry (VLBI) measurements (dotted). For example, the coincident fraction calculated using GW parameter estimation and VLBI measurements for a Gaussian jet model is given by the violet dotted line. From this curve, we see that we would expect a coincident detection 70% of the time if $\theta_B \gtrsim 5°$ in the Gaussian jet model. We see that the exclusion of small θ_B becomes more certain as parameter estimation results provide more precise measurements of the viewing angle. Indeed, the measurement using VLBI confidently rules out jet widths less than 14° for broken power-law and tophat models. As seen in the black and orange dotted curves, the probability for coincident detection is <0.01 for $\theta_B < 14°$; given that GRB 170817A was seen, this strongly disfavors these low jet widths. Please note that the precise meaning of θ_B depends on the jet structure model and constraints on θ_B may not be directly comparable between models (see Figure 4). The broken power-law model produces a coincident fraction that closely follows that of the tophat jet for all three examined data sources. This indicates that the truncation at θ_B for the tophat model is the relevant feature for this analysis, rather than the fall off in the region $\theta_B/2 < \iota < \theta_B$.

We note that the numerator can be written as

$$\begin{aligned} p(d_i, \mathcal{A}^{(i)}_{\rm coinc}, \mathcal{A}^{(i)}_{\rm GW} = 1|\theta_B) &= \int {\rm d}z{\rm d}\iota\, p(z, \iota) \\ &\times p(d_i, \mathcal{A}^{(i)}_{\rm GW} = 1|z, \iota) p(\mathcal{A}^{(i)}_{\rm coinc}|z, \iota, \theta_B) \\ &= \int {\rm d}z{\rm d}\iota (p(z, \iota|d_i, \mathcal{A}^{(i)}_{\rm GW} = 1) \\ &\times p(d_i, \mathcal{A}^{(i)}_{\rm GW} = 1) p(\mathcal{A}^{(i)}_{\rm coinc}|z, \iota, \theta_B), \end{aligned} \tag{12}$$

so that

$$\begin{aligned} q_i = \int {\rm d}z_i {\rm d}\iota_i\, p(z_i, \iota_i|d_i, \mathcal{A}^{(i)}_{\rm GW} = 1) \\ \times p(\mathcal{A}^{(i)}_{\rm coinc}|z_i, \iota_i, \theta_B). \end{aligned} \tag{13}$$

Note that $p(z, \iota|d_i, \mathcal{A}^{(i)}_{\rm GW} = 1)$ is simply the GW posterior on inclination and redshift, so we can compute q_i by Monte-Carlo sampling $p(\mathcal{A}_{\rm coinc}|z, \iota; \theta_B)$ from the GW posterior. We can thus think of $p(z, \iota|d_i, \mathcal{A}^{(i)}_{\rm GW} = 1)$ obtained from GW data as our new prior on z and ι for this event.

Because the overall rate of BNS mergers is unknown, a joint analysis of multiple events would need to explicitly account for the selection effects associated with different possible merger rates throughout the universe. As is common in the GW literature (e.g., Loredo 2004; Abbott et al. 2019b; Mandel et al. 2019; Fishbach & Holz 2020), we can adopt an inhomgeneous Poisson likelihood

$$\begin{aligned} &p(\{d_i, \mathcal{A}^{(i)}_{\rm GW}, \mathcal{A}^{(i)}_{\rm coinc}\}) \\ &= \left[\prod_i^{N_{\rm GW}} \int {\rm d}z{\rm d}\iota\, p(z, \iota) p(d_i|z, \iota, \mathcal{A}^{(i)}_{\rm GW})\ \ p(\mathcal{A}^{(i)}_{\rm coinc}|z, \iota)\right] e^{-\mathcal{N}}, \end{aligned} \tag{14}$$

where $\mathcal{N}$ is the expected number of detections given the population described by $p(z, \iota)$ implicitly included in each q_i and an overall merger rate. By again considering the probability of detecting sGRBs given the knowledge of GW detections, we obtain the following joint likelihood

$$\begin{aligned} \Lambda &= p(\{\mathcal{A}^{(i)}_{\rm coinc}\}|\{d_i, \mathcal{A}^{(i)}_{\rm GW}\}) = \frac{p(\{d_i, \mathcal{A}^{(i)}_{\rm GW}, \mathcal{A}^{(i)}_{\rm coinc}\})}{p(\{d_i, \mathcal{A}^{(i)}_{\rm GW}\})} \\ &= \frac{\left[\prod \int {\rm d}z{\rm d}\iota\, p(z, \iota) p(d_i|z, \iota, \mathcal{A}^{(i)}_{\rm GW}) p(\mathcal{A}^{(i)}_{\rm coinc}|z, \iota)\right] e^{-\mathcal{N}}}{\left[\prod \int {\rm d}z{\rm d}\iota\, p(z, \iota) p(d_i|z, \iota, \mathcal{A}^{(i)}_{\rm GW})\right] e^{-\mathcal{N}}} \\ &= \prod_i^{N_{\rm GW}} q_i. \end{aligned} \tag{15}$$

This means that our inference about jet parameters is insensitive to the overall rate of mergers in the universe since we condition on the fact that the system was detected in GWs, although we are still sensitive to the distribution of mergers throughout the universe through the implicit dependence on $p(z, \iota)$ contained in each q_i.

As an example, if there were two gravitational-wave events and only one of them had a coincident sGRB detection, we would have

$$\begin{aligned} \Lambda = p(d_1, \mathcal{A}^{(1)}_{\rm coinc} = 1|\mathcal{A}^{(1)}_{\rm GW} = 1, \theta_B) \\ \times p(d_2, \mathcal{A}^{(2)}_{\rm coinc} = 0|\mathcal{A}^{(2)}_{\rm GW} = 1, \theta_B), \end{aligned} \tag{16}$$

which is a natural generalization of the binomial distribution, as the first factor is analogous to q, and the second to $1 - q$.

3. Results

To date there have been two BNS events detected in GWs (Abbott et al. 2017b, 2020), one of which was accompanied by an sGRB (Goldstein et al. 2017). In this section, we first discuss the implications of this fact using the counting experiment formalism described in Section 2.2. We will then present how these results differ when we take advantage of information provided by both GW parameter estimation and very long baseline interferometry (VLBI) measurements of inclination (Mooley et al. 2018; Hotokezaka et al. 2019). Finally, we provide predictions for the future constraining power given various numbers of GW and sGRB detections.

3.1. Counting Experiment with GW170817

If $N_{\rm GW} = N_{\rm coinc} = 1$, Equation (2) simplifies to $p(\theta_B|N_{\rm GW} = 1, N_{\rm coinc} = 1) \propto q(\theta_B)$. Figure 3 shows the coincident fraction, proportional to the posterior probability for one event, as a function of θ_B based on the counting experiment. For all jet

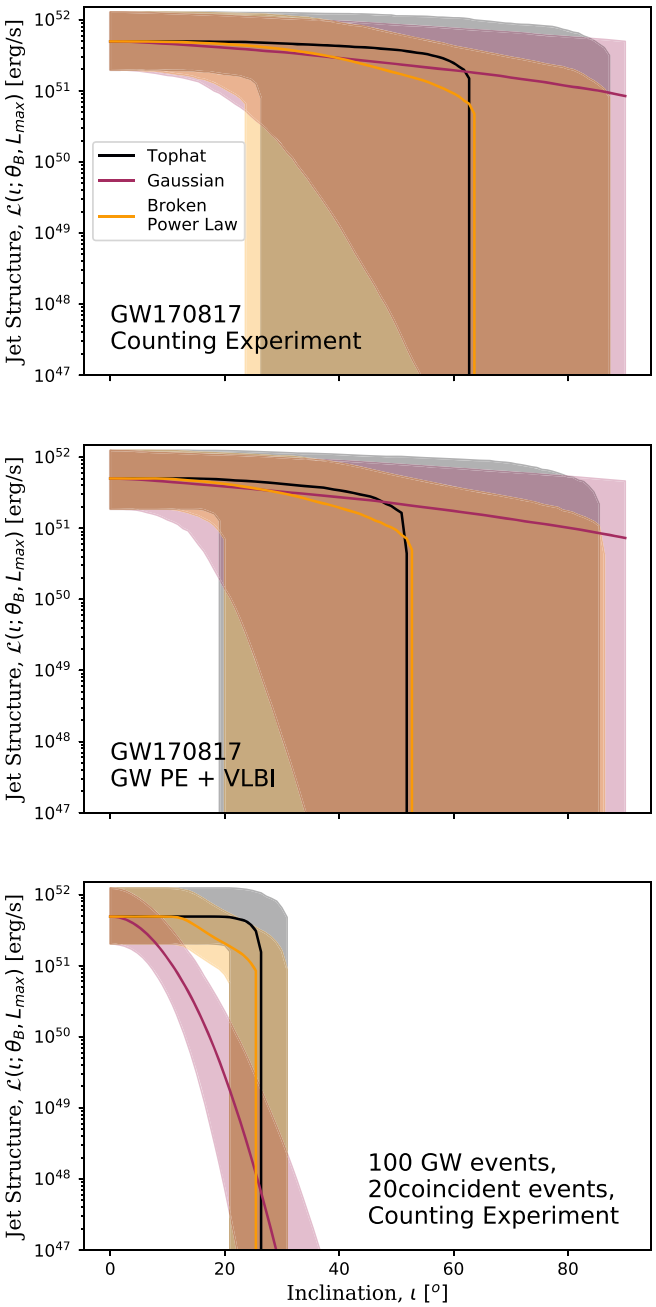

Figure 4. Uncertainty in jet structure with the tophat (black), broken power-law (orange), and Gaussian (violet) models. Top: constraints from the counting experiment with GW170817 alone. Middle: constraints from GW170817 including GW parameter estimation and the precise determination of the viewing angle from VLBI measurements. Bottom: expected constraints from the counting experiment alone after 100 GW events with 20 coincident sGRBs. We note that the constraints obtained from GW170817 are nearly identical regardless of whether we perform a simple counting experiment or use the full set of available parameter estimations. As such, we only show the expected constraints after 100 GW events with the counting experiment because it is indistinguishable from the expectation with simulated GW parameter estimation.

structures considered, this rules out $\theta_B \approx 0$ and favors large jet widths, which is to be expected since 100% of BNS detections have been accompanied by an sGRB.

For a tophat jet structure, θ_B is the angular width of the uniform portion (Equation (6)). At inclinations beyond θ_B, gamma-rays do not reach GBM. Since an sGRB was detected, the tophat model has the most support for $\theta_B = 90°$. However, because there is significant uncertainty in the viewing angle based on GW selection effects alone, there is rather broad support for many θ_B. For the broken power-law model, θ_B is the inclination at which the luminosity goes to zero (Equation (8)). It is also twice the angular width of the uniform core. The coincident fraction in this case traces that of the tophat jet, indicating that the truncation at θ_B is the dominant feature, rather than the fall off in the region $\theta_B/2 < \iota < \theta_B$. Recall that the exponent in the power-law region was chosen to be -2, but larger negative powers up to -5 were explored, and did not have noticeable impacts on the results. Additionally, truncating the power law at $\iota = 90°$ instead of at $\iota = \theta_B$ yielded results similar to those of the Gaussian jet. The differences in constraints on θ_B between models, then, is primarily an artifact of how we parameterized the models. Figure 4 shows the uncertainty in the luminosity distribution itself, and we see that the actual model dependence is much smaller than Figure 3 might suggest. For a Gaussian jet structure, recall that we define θ_B as the standard deviation (Equation (7)). Since the Gaussian jet has wide tails, it allows for relatively high luminosities at all inclinations even with a small standard deviation, leading to more support for lower θ_B. If we instead define θ_B to be four times the standard deviation, such that the luminosity at θ_B is approximately four orders of magnitude lower than at the center of the jet, then the coincident fraction for a Gaussian jet closely traces those of the broken power-law and tophat models for equivalent values of θ_B. This is because, for the majority of events seen in GWs, the isotropic luminosity threshold is $\sim 10^{48}$ erg s^{-1} (Figure 1), which is approximately four orders of magnitude lower than typical values of $L_{\rm max}$. Parameterizing the Gaussian model using $\theta_B = 4\sigma$ instead of $\theta_B = 1\sigma$ does not affect the inference on the jet structure, but would make θ_B the point at which the luminosity of the jet crosses GBM's isotropic luminosity threshold, and hence more analogous to the meaning of θ_B for the other models.

3.2. GW170817 Posteriors and sGRB Structure

Using parameter estimation from GW170817 obtained from Abbott et al. (2019a) changes this measurement somewhat. Slightly tighter constraints on inclination angle and redshift nearly rule out that the system is edge-on, so a 90° jet opening angle is not as necessary to explain the fact that gamma-rays were observed. However, 90° jets are still consistent with the data. This allows for slightly more support for medium-width jets ($\theta_B \sim 45°$–$70°$) than is provided from the simple counting experiment, demonstrated in Figure 3. However, this improvement is marginal even for loud events because inclination and distance are degenerate and thus cannot be determined to high precision separately, apart from what is known about their impact on LIGO's sensitivity. Only extreme outliers will lead to strong constraints on the inclination from the GW data alone (Chen et al. 2019). In this way, the counting experiment method is rather powerful because most of the information about a GW event's inclination and redshift is provided by the fact that it was detected.

When an external measurement is used to break the inclination-distance degeneracy, such as a redshift from identification of a host galaxy, or the inclination from superluminal motion of the radio afterglow of an sGRB (Hotokezaka et al. 2019), constraints are much improved. In the case of GW170817, Hotokezaka et al. (2019) find the

inclination to be between $\sim 14^\circ$ and $\sim 19^\circ$. Given that an sGRB was observed, this implies that the beaming angle must be larger than the lower bound of this region for the tophat case. The broken power-law result traces that of the tophat, and the Gaussian result strictly favors $\theta_B > 4^\circ$. Again, these differences reflect parameterization choices. Figure 4 shows the uncertainty in $\mathcal{L}(\iota)$.

Nonetheless, as with the simple counting experiment, the posteriors on θ_B are essentially sigmoids of varying steepness. Tighter constraints on the inclination for individual events will make these curves somewhat steeper, but their general morphology will remain the same. We note, then, that combining information from multiple events will be equivalent to multiplying sigmoids. Detections of sGRBs will exclude small θ_B and nondetections will exclude larger θ_B, producing a narrow window of posterior probability around the true value. We explore this further in the context of multiple detections below.

3.3. GW190425 Posteriors and sGRB Structure

The recent detection of GW190425 in gravitational waves (Abbott et al. 2020) was not associated with an accompanying sGRB. Under the assumption that GW190425 is a BNS coalescence, the nondetection of an electromagnetic counterpart provides further insight on the jet structure of sGRBs. A recent analysis by Coughlin et al. (2019) has similarly taken advantage of nondetections of electromagnetic counterparts of several additional event candidates by using expected optical and infrared light curves from kilonova modeling to constrain the mass ejected from BNS coalescences.

The current scenario of two BNS coalescences detected in GWs with only one accompanied by an sGRB is described by Equation (16). We therefore denote data obtained using gravitational-wave parameter estimation for GW170817 and GW190425 as d_1 and d_2, respectively. Data from GW190425 is not informative on inclination and redshift as it was a single-detector event. Thus, the coincident fraction for GW190425 computed using parameter estimation is nearly identical to that calculated using the counting experiment method. As such, the joint likelihood Λ is largely similar to the numerator in Equation (2) with $N_{\rm GW} = 2$ and $N_{\rm coinc} = 1$.

In Figure 5, we show the individual event likelihoods for GW170817 and GW190425 along with their joint likelihood. From this, we note that the addition of information from GW190425 produces a joint likelihood with more support for $25^\circ \lesssim \theta_B \lesssim 60^\circ$, and less support at very high angles when compared with the individual event likelihood from GW170817 alone. The joint likelihood is still largely uninformative, though it demonstrates an improvement in precision with the addition of more events.

3.4. Projected Constraints with Future Events

In the future, LIGO and Virgo will detect many more BNS systems. Given the detection of one event in O2 and increased sensitivity in O3, it is possible that several new mergers will be detected by the end of O3 (Abbott et al. 2018). Thus, we generate posteriors for $N_{\rm GW} = 5$ and various $N_{\rm coinc}$ using the coincident fractions for the three jet structures considered here (Figure 3). We note that sources detected in GWs are detected at fairly low redshift, and the mean of the distribution from which $L_{\rm max}$ is drawn is high enough that the $L_{\rm max}$ of any given event is still orders of magnitude higher than the isotropic luminosity threshold for GBM (Figure 1). Thus, jet structure will not bring many events below that threshold, even at high inclination. As such, we show an example of the constraints on a tophat jet obtained from a counting experiment with 5 and 100 GW detections in Figure 6. With 100 detections, θ_B will be constrained to within 3° for the tophat model if $N_{\rm coinc} = 20$. We illustrate implications of these constraints on inferred jet structure in Figure 4. In the case of 100 BNS systems detected in GWs, with 20 of them being coincident with sGRBs, we transform the posterior on θ_B into a 90% confidence region of luminosity as a function of inclination for each jet structure model.

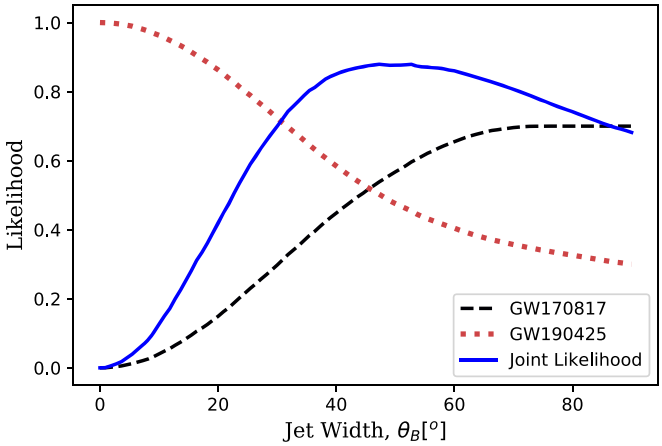

Figure 5. Individual event likelihoods of θ_B for GW170817 $p(d_1, \mathcal{A}^{(1)}_{\rm coinc} = 1|\mathcal{A}^{(1)}_{\rm GW} = 1, \theta_B)$ (black dashed) and GW190425 $p(d_2, \mathcal{A}^{(2)}_{\rm coinc} = 0|\mathcal{A}^{(2)}_{\rm GW} = 1, \theta_B)$ (magenta dotted), along with their joint likelihood Λ (blue solid), assuming a tophat jet structure. For comparison, note that the black dashed curve here is identical to the black dashed curve in Figure 3. While each individual likelihood peaks at a different beaming angle, the joint likelihood is more constraining and peaks near $\theta_B = 47^\circ$.

While there is a clear model dependence on these credible intervals within the jet, all these models agree that there is essentially no emission beyond $\sim 30^\circ$ in this simulation. The three models overlap at $\iota \sim 25^\circ$, which corresponds to an isotropic equivalent luminosity of $\sim 10^{48}$ erg s^{-1}. This is because GBM's isotropic luminosity threshold is close to this value for most sources considered (see Figure 1), as most of the simulated events' redshifts are above $z \sim 0.01$. From this, we see that the method outlined in this work primarily constrains the redshift-averaged viewing angle beyond which no sGRBs are observed by GBM, given a detection in gravitational waves. This angle can be thought of as an "effective beaming angle," and it depends on the distribution chosen for $L_{\rm max}$, as well as the sensitivity of the instrument used to observe gamma-rays. Modeling systematics may then affect the inference of jet structure, but they will not strongly influence our first-order conclusions, like whether there is significant emission outside of a narrow window.

Including GW parameter estimation, however, modifies the likelihood. Although improvements are small in the individual event case, with many events this could significantly impact the overall likelihood of the jet width. To get a sense of how this will change with real events, mock parameter estimation posteriors are created using the relation between true inclination and inclination uncertainty presented in Figure 4 of Chen et al. (2019). We simulate 100 BNS merger events with a range

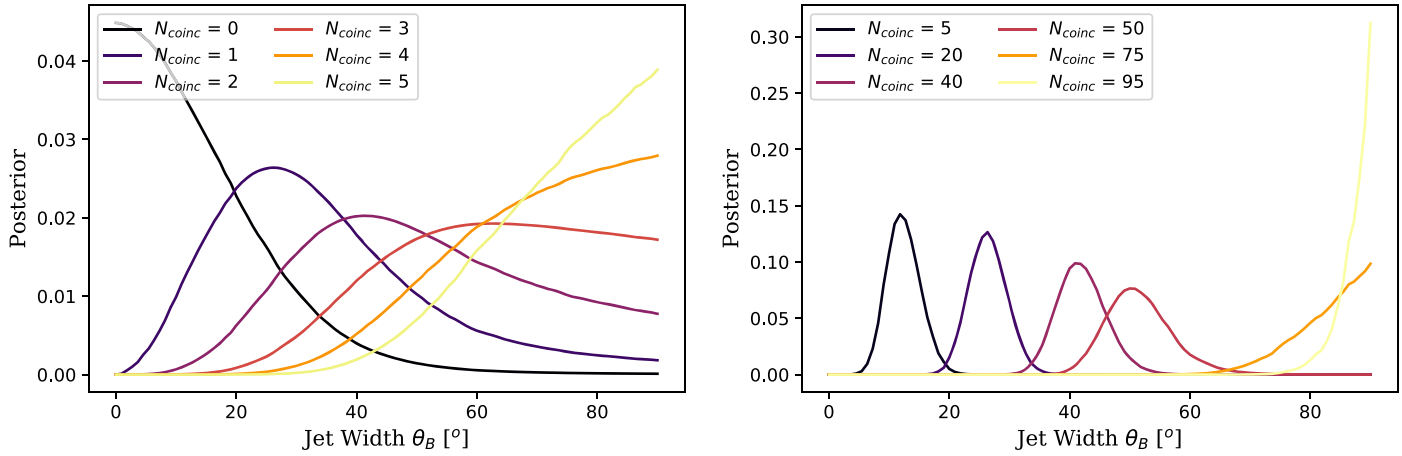

Figure 6. Potential future constraints from our counting experiment for (left) 5 and (right) 100 BNS systems detected in GWs, given the tophat jet model. We generally obtain tighter constraints with more events and note that the improvement from GW parameter estimation will become negligible after ∼100 BNS detections.

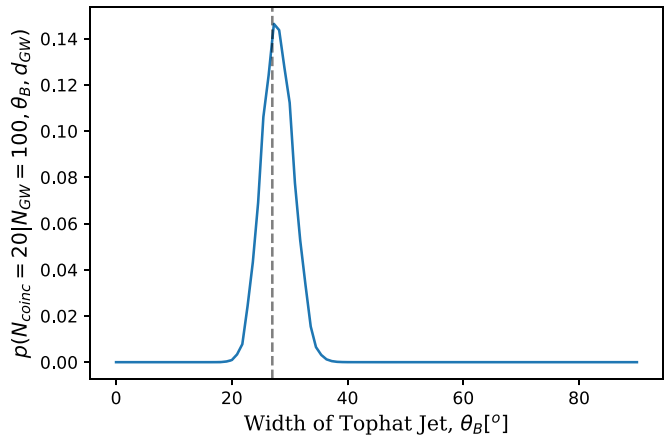

Figure 7. Total likelihood with simulated GW parameter estimation for the case of 100 events with a tophat jet. In this simulation, $\theta_B = 27°$ (vertical dashed gray line), within the expected uncertainty from the posterior. This true value is chosen for easy comparison with the $N_{\rm GW} = 100$, $N_{\rm coinc} = 20$ result from the counting experiment (orange curve in right panel of Figure 7). We note that the uncertainty in θ_B is comparable to what is achieved by the simple counting experiment with the same number of events.

of beaming angles. This is shown in Figure 7. Note that these projections for future constraints on θ_B are conservative in the sense that they are calculated under the assumption that neither VLBI observations nor host galaxy identification are available.

GW parameter estimation can significantly improve the constraints on θ_B with only a few events, but it produces nearly identical constraints compared to the simpler counting experiment in the limit of many detections. This is because the individual event likelihoods are sigmoids, and the product of multiple sigmoids is still a sigmoid. As discussed in Section 3.2, parameter estimation can make the individual event likelihoods steeper than what is produced by the counting experiment, and this leads to an overall tighter constraint, particularly with a small number of events. However, the joint posterior will be dominated by the single event with the largest (smallest) well-constrained viewing angle that is smaller (larger) than the true θ_B and does (does not) have an associated sGRB. This means constraints will tighten rapidly with the first few events, but will eventually require a large number of detections to obtain an outlier with large (small) enough θ_B to further improve our knowledge.

While the counting experiment produces smoother single-event posteriors, we note that the product of many smooth sigmoids is a relatively sharp sigmoid. Therefore, parameter estimation's initial advantage can be overcome with many events, and the constraints obtained by both approaches will be quite similar after 100 BNS detections. It is really the overall sensitivities and angular scales associated with GW and sGRB emission and detection, as encoded in simple counting experiments, that drive our ability to constrain the beaming angle with many events.

4. Discussion

We present two methods to determine the width of an sGRB jet assuming a specific universal jet structure. We showed that with 100 BNS detections in GWs, a simple counting experiment will constrain θ_B to 12%, and including GW parameter estimation will constrain θ_B to within 9.6% assuming a tophat jet structure. The methods presented here are complementary to light curve jet-break measurements of inclination, and a comparison between the two might provide an interesting test of the existence of a universal jet structure. While our counting constraints on θ_B may not be extremely informative by the end of O3, compared to those obtained through jet-break measurements, our method is relatively straightforward, robust, and does not require lengthy electromagnetic observations. It also infers similar jet widths for all models considered here. As such, it provides a useful comparison and basic sanity check of our models.

It is also important to emphasize that none of the jet structure models considered here easily produce an event that is observed as subluminously as GRB 170817A ($\sim 10^{47}$ erg s^{-1}; Abbott et al. 2017a). This is because, as mentioned previously, $L_{\rm max}$ is drawn from a relatively narrow distribution that is peaked at a luminosity orders of magnitude higher than that of GW170817. While that distribution was picked to be consistent with the majority of observed sGRBs with known redshift, it may still be flawed, and future work will explore the consequences of drawing $L_{\rm max}$ from a wider distribution. Alternatively, one could simultaneously constrain θ_B and $L_{\rm max}$,

or choose jet structure models that fall off more steeply with increasing inclination than Gaussian or broken power-law models but do not actually vanish.

Another important caveat is that, as mentioned in Section 1, in order to do such a calculation one must assume a universal jet structure. It is likely that this is not the case, as the jet structure could depend on the physical properties of the BNS system and circumburst environment. One natural way to account for this would be to constrain the distribution of θ_B; that is, model each BNS system with a separate θ_B but require them all to be drawn from a single distribution. Such an approach would produce a family of parameterized jet structures and assign a relative likelihood to each:

$$\Lambda(\lambda) = \prod_{i}^{N_{\rm GW}} \int d\theta_B p(\theta_B|\lambda) q_i(\theta_B), \tag{17}$$

where $p(\theta_B|\lambda)$ describes the relative probability of obtaining different θ_B, described by the parameters λ. However, this also requires us to assume a particular parameterization of the jet structure, which may be difficult to extract from simulations. If the fidelity of parameterized models is difficult to verify, one might pursue a nonparametric approach instead. In such approaches, no specific functional form is assumed for the jet structure but instead we rely on the data alone to determine correlations between the luminosity at various viewing angles. Gaussian processes provide a natural formalism for such an inference scheme and have been pursued in similar contexts within the GW literature (e.g., Landry & Essick 2019; Essick et al. 2020). Specifically, one would replace the implicit distribution over $\mathcal{L}$ described by $p(\theta_B|\lambda)$ with a Gaussian process for $\mathcal{L}$. If there is a universal jet structure, the nonparametric posterior process for $\mathcal{L}$ should collapse to a single curve, regardless of the true jet structure's functional form. If the jet structure is not universal, then the nonparametric posterior process will capture the full variability of the jets produced in nature, again regardless of their precise functional form. Similar techniques have been proposed for parameterized tests of general relativity with GW events (Isi et al. 2019). Such a nonparametric analysis would avoid modeling errors associated with choosing a functional form for the jet structure a priori, and instead would infer the full distribution of jet structures observed in nature directly from the data. However, we note that sampling from such nonparametric posterior processes can be nontrivial and leave further exploration to future work.

At present, statistical uncertainty dominates systematic modeling errors with GW170817 and GW190425. We find that the majority of the constraining power of GWs for sGRB jet widths results from the relative sensitivity to sources at different redshift and inclination in both GW detectors and GBM. We demonstrate that our simple counting experiment can determine the jet width to nearly the same precision as more complex approaches that rely on computationally expensive parameter estimation techniques. We also illustrate the simple extension of our approach to use gravitational-wave and electromagnetic parameter estimation, which will more quickly constrain the geometry of sGRBs with a small number of detections but will not significantly improve over counting experiments after $\sim$100 BNS detections. As such, we can count on sGRBs detected in coincidence with GW events to help us constrain the angular emission profile of all sGRBs, from which we can develop a better understanding of the physical processes driving sGRB jets and the remnants of compact binary mergers.

The authors are grateful to Edo Berger, Cecelia Chirenti, Ryan Foley, Wen-Fai Fong, Chris Fryer, Dan Kasen, Raffaella Margutti, Brian Metzger, Cole Miller, and Karelle Siellez for helpful discussions about gamma-ray bursts. We also thank Karelle Siellez and Eric Thrane for useful conversations about GBM, and for sharing methodologies used to compute GBM's isotropic luminosity threshold. We thank the LIGO Scientific Collaboration and Virgo Collaboration for public access to data products. This research was conducted in part at the Kavli Institute for Theoretical Physics, supported in part by the National Science Foundation under grant No. NSF PHY-1748958. A.F., R.E., M.F., Z.D., and D.E.H. were supported by the Kavli Institute for Cosmological Physics at the University of Chicago through NSF grant PHY-1125897 and an endowment from the Kavli Foundation. A.F., M.F., Z.D., and D.E.H. were also supported by NSF grant PHY-1708081. M.F. and Z.D. were supported by the NSF Graduate Research Fellowship Program under grants DGE-1746045 and DGE-1144082, respectively. D.E.H. also gratefully acknowledges support from the Marion and Stuart Rice Award.

ORCID iDs

Amanda Farah https://orcid.org/0000-0002-6121-0285
Reed Essick https://orcid.org/0000-0001-8196-9267
Zoheyr Doctor https://orcid.org/0000-0002-2077-4914
Maya Fishbach https://orcid.org/0000-0002-1980-5293
Daniel E. Holz https://orcid.org/0000-0002-0175-5064

References

Aasi, J., Abbott, B. P., Abbott, R., et al. 2015, CQGra, 32, 074001
Abbott, B., Abbott, R., Abbott, T., et al. 2019a, PhRvX, 9, 031040
Abbott, B. P., Abbott, R., Abbott, T. D., et al. 2017a, ApJL, 848, L13
Abbott, B. P., Abbott, R., Abbott, T. D., et al. 2017b, PhRvL, 119, 161101
Abbott, B. P., Abbott, R., Abbott, T. D., et al. 2018, LRR, 21, 3
Abbott, B. P., Abbott, R., Abbott, T. D., et al. 2019b, ApJL, 882, L24
Abbott, B. P., Abbott, R., Abbott, T. D., et al. 2020, ApJL, 892, L3
Acernese, F., Agathos, M., Agatsuma, K., et al. 2015, CQGra, 32, 024001
Aloy, M. A., Janka, H. T., & Müller, E. 2005, A&A, 436, 273
Aptekar, R. L., Frederiks, D. D., Golenetskii, S. V., et al. 1995, SSRv, 71, 265
Berger, E. 2014, ARA&A, 52, 43
Biscoveanu, S., Thrane, E., & Vitale, S. 2020, ApJ, 893, 38
Blandford, R. D., & McKee, C. F. 1976, PhFl, 19, 1130
Burns, E., Connaughton, V., Zhang, B.-B., et al. 2016, ApJ, 818, 110
Chen, H.-Y., & Holz, D. E. 2013, PhRvL, 111, 181101
Chen, H.-Y., Vitale, S., & Narayan, R. 2019, PhRvX, 9, 031028
Church, R. P., Levan, A. J., Davies, M. B., & Tanvir, N. 2011, MNRAS, 413, 2004
Coughlin, M. W., Dietrich, T., Antier, S., et al. 2019, MNRAS, 492, 863
Eichler, D., Livio, M., Piran, T., & Schramm, D. N. 1989, Natur, 340, 126
Essick, R., Landry, P., & Holz, D. E. 2020, PhRvD, 101, 063007
Finn, L. S., & Chernoff, D. F. 1993, PhRvD, 47, 2198
Fishbach, M., & Holz, D. E. 2020, ApJL, 891, L27
Fong, W., Berger, E., & Fox, D. B. 2010, ApJ, 708, 9
Fong, W., Berger, E., Margutti, R., & Zauderer, B. A. 2015, ApJ, 815, 102
Frail, D. A., Kulkarni, S. R., Sari, R., et al. 2001, ApJL, 562, L55
Gehrels, N., Chincarini, G., Giommi, P., et al. 2004, ApJ, 611, 1005
Ghirlanda, G., Salafia, O. S., Pescalli, A., et al. 2016, A&A, 594, A84
Gill, R., & Granot, J. 2018, MNRAS, 478, 4128
Goldstein, A., Veres, P., Burns, E., et al. 2017, ApJL, 848, L14
Hayes, F., Heng, I. S., Veitch, J., & Williams, D. 2020, ApJ, 891, 124

Hotokezaka, K., Nakar, E., Gottlieb, O., et al. 2019, NatAs, 3, 940
Isi, M., Chatziioannou, K., & Farr, W. M. 2019, PhRvL, 123, 121101
Jin, Z.-P., Li, X., Wang, H., et al. 2018, ApJ, 857, 128
Kumar, P., & Zhang, B. 2015, PhR, 561, 1
Landry, P., & Essick, R. 2019, PhRvD, 99, 084049
Laskar, T., Alexander, K. D., Berger, E., et al. 2016, ApJ, 833, 88
Laskar, T., Berger, E., Chornock, R., et al. 2018, ApJ, 858, 65
Lazzati, D., Deich, A., Morsony, B. J., & Workman, J. C. 2017, MNRAS, 471, 1652
Liu, T., Hou, S.-J., Xue, L., & Gu, W.-M. 2015, ApJS, 218, 12
Loredo, T. J. 2004, in AIP Conf. Proc. 735, 24th International Workshop on Bayesian Inference and Maximum Entropy Methods in Science and Engineering, ed. R. Fischer, R. Preuss, & U. V. Toussiant (Melville, NY: AIP), 195
Lyman, J. D., Lamb, G. P., Levan, A. J., et al. 2018, NatAs, 2, 751
Mandel, I., Farr, W. M., & Gair, J. R. 2019, MNRAS, 486, 1086
Meegan, C., Lichti, G., Bhat, P. N., et al. 2009, ApJ, 702, 791
Metzger, B. D., & Berger, E. 2012, ApJ, 746, 48
Mogushi, K., Cavaglià, M., & Siellez, K. 2019, ApJ, 880, 55
Mooley, K. P., Deller, A. T., Gottlieb, O., et al. 2018, Natur, 561, 355
Nagakura, H., Hotokezaka, K., Sekiguchi, Y., Shibata, M., & Ioka, K. 2014, ApJL, 784, L28
Nakar, E., Granot, J., & Guetta, D. 2004, ApJL, 606, L37
Narayan, R., Paczynski, B., & Piran, T. 1992, ApJL, 395, L83
Perna, R., Sari, R., & Frail, D. 2003, ApJ, 594, 379
Salafia, O. S., Ghisellini, G., Pescalli, A., Ghirland, A. G., & Nappo, F. 2015, MNRAS, 450, 3549
Savchenko, V., Ferrigno, C., Kuulkers, E., et al. 2017, ApJL, 848, L15
Siellez, K., Boer, M., Gendre, B., & Regimbau, T. 2016, arXiv:1606.03043
Suzuki, A., & Shigeyama, T. 2014, ApJ, 796, 30
The LIGO Scientific Collaboration 2019, Gravitational-Wave Observatory Status (Hanford Site, WA: Gravitational-Wave Observatory), https://www.gw-openscience.org/detector_status/
Wanderman, D., & Piran, T. 2015, MNRAS, 448, 3026
Wang, X.-G., Zhang, B., Liang, E.-W., et al. 2018, ApJ, 859, 160
Wu, Y., & MacFadyen, A. 2019, ApJL, 880, L23
Yi, S.-X., Lei, W.-H., Zhang, B., et al. 2017, JHEAp, 13, 1
Zhang, B. 2016, ApJL, 822, L14
Zhang, B., & Mészáros, P. 2002, ApJ, 571, 876
Zou, Y.-C., Wang, F.-F., Moharana, R., et al. 2018, ApJL, 852, L1